Dynamical drivers of Greenland blocking in climate models

Clio Michel*[1], Erica Madonna*[1], Clemens Spensberger[1], Camille Li[1], and Stephen Outten[2]

[1]Geophysical Institute, University of Bergen and Bjerknes Centre for Climate Research, Bergen, Norway
[2]Nansen Environmental and Remote Sensing Center and Bjerknes Center for Climate Research, Bergen, Norway
*The authors equally contributed to the study

Correspondence: Clio Michel (Clio.Michel@uib.no)

Abstract. Blocking over Greenland is known to lead to strong surface impacts, such as ice sheet melting, and a change in its future frequency can have important consequences. However, as previous studies demonstrated, climate models underestimate the blocking frequency for the historical period. Even though some improvements have recently been made, the reasons for the model biases are still unclear. This study investigates whether models with realistic Greenland blocking frequency in winter have a correct representation of its dynamical drivers, most importantly, cyclonic wave breaking (CWB). Because blocking is a rare event and its representation is model-dependent, we here use a multi-model large ensemble. ~~All of the models~~ We focus on two models that both underestimate CWB frequency ~~and four out of five models underestimate the frequency of Greenland blocking~~ but with different representation of the wintertime Greenland blocking frequency. Nevertheless, they ~~all~~ both show the typical Greenland blocking features, namely a ridge with anticyclonic anomaly over Greenland and an equatorward-shifted jet over the North Atlantic. However, we find that the model with the most realistic Greenland blocking frequency, MIROC5, has the most negative CWB frequency bias. While in reanalysis CWB is an important mechanism leading to blocking formation, the link between blocking and CWB is much weaker in MIROC5, suggesting that another mechanism leads to blocking in this model. Composites over Greenland blocking days show that the present and future experiments of each model are very similar to each other in both amplitude and pattern and that there is no significant change of Greenland blocking frequency in the future. However, this result must be taken with caution since the Greenland blocking driver is not well represented in all models. This highlights the need to accurately understand and represent the mechanisms leading to blocking formation and maintenance in models to get more reliable future projections.

1 Introduction

Blocking in the atmosphere is a persistent quasi-stationary anticyclonic anomaly that disrupts the westerly flow (Rex, 1950). Often occurring in mid-latitude regions such as Greenland and Europe/Scandinavia (Treidl et al., 1981; Davini et al., 2014), it has profound impacts on surface weather, leading to temperature extremes such as cold spells in winter (Trigo et al., 2004; Sillmann and Croci-Maspoli, 2009) and heat waves in summer (Pfahl and Wernli, 2012; Schaller et al., 2018). Blocking over Greenland is shown to last longer than blocking over other regions (e.g, Davini et al., 2012; Drouard et al., 2021). Moreover, Greenland blocking has been shown to cause melting events of the Greenland Ice Sheet ~~(Fettweis et al., 2013; McLeod and Mote, 2015; Hanna et al., 2021; Hermann et al., 2020),~~

(Fettweis et al., 2013; McLeod and Mote, 2015; Hermann et al., 2020; Hanna et al., 2021), by mainly reducing the cloud cover, increasing temperatures (Chen and Luo, 2017), and changing the surface energy budget (Ward et al., 2020, and references therein) , which can impact global sea level rise (Van den Broeke et al., 2016). In addition to the local impact, Greenland blocking is also associated with temperature anomalies over the whole Northern Hemisphere (Chen and Luo, 2017). It is therefore crucial that models correctly represent blocking in order to accurately simulate its impacts and potential future changes. Unfortunately, blocking frequency over the North Atlantic is still underestimated by the large majority of climate models despite some improvements in recent years (see Davini and D'Andrea, 2020, for a review). Moreover, as blocking events are also sporadic and exhibit a large natural variability (Woollings et al., 2018), some models will not simulate enough blocking events to robustly investigate the mechanisms leading to blocking, hence the need for very long simulations or many different realizations of the same experiment. In the present study, we make use of large ensembles of climate models with relatively coarse spatial resolutions that provide a broad sampling of the internal variability of the atmosphere to investigate the biases in Greenland blocking and the dynamical driving from Rossby wave breaking (RWB). Moreover, knowing these biases, we will look at how changes in RWB in a 2°C warmer world will shape future Greenland blocking frequency and pattern.

Climate models have steadily improved over the last decades but still struggle to correctly represent some important features of the atmospheric circulation such as the jet stream, the storm tracks, and the blocking over both the North Pacific and Atlantic. In the North Atlantic, the jet streams and storm tracks produced by the climate models from the various phases of the ~~Climate~~ Coupled Model Intercomparison Project (CMIP) continue to be too zonal and placed too far south compared to reanalyses (Harvey et al., 2020). Most CMIP5 models do not reproduce the observed blocking frequency in the North Atlantic sector (Vial and Osborn, 2012; Masato et al., 2013; Anstey et al., 2013; Davini and D'Andrea, 2016) with up to a 30–50% underestimation of wintertime blocking frequencies (Woollings et al., 2018). Similar blocking biases are found in uncoupled climate models (e.g. Davini and D'Andrea, 2016). Many of the new generation models (CMIP6) show an improvement in reproducing blocking frequencies, but for some regions, such as the North Atlantic, most still have too little blocking (Davini and D'Andrea, 2020; Schiemann et al., 2020). Some studies have ~~showed~~ shown that statistically correcting the model's mean state improves the overall frequency of blocking and that a blocking detection method based on anomalies might be less sensitive to mean state biases compared to a method based on the meridional reversal of the geopotential gradient (Scaife et al., 2010; Vial and Osborn, 2012). However, Schiemann et al. (2020) showed that using an anomaly threshold does not necessarily remove the general blocking biases.

Many studies have documented model biases, but only some have tried to understand the physical drivers. For example, several studies have reported that biases in blocking are associated with biases in the mean flow (Scaife et al., 2010; Vial and Osborn, 2012) but have not further explored potential mechanisms linking the mean state to the occurrence of blocking. Other studies have reported a general decrease of North Atlantic blocking bias with increased model resolution (Anstey et al., 2013; Davini and D'Andrea, 2016; Davini et al., 2017; Schiemann et al., 2017; Davini and D'Andrea, 2020; Schiemann et al., 2020). With increased resolution comes a better representation of the orography, which in turn improves the mean state (e.g. the stationary wave patterns) and variability. Through this mechanism increased resolution can reduce blocking biases, but the benefits vary regionally (Berckmans et al., 2013; Davini et al., 2017). Similarly, Pithan et al. (2016) showed

that a better parameterisation of orographic drag improved the blocking representation over the North Atlantic, but had the opposite effect over the North Pacific. Finally, Davini et al. (2017) found that realistic blocking frequencies may result from bias compensations: overly strong eddies at upper levels counterbalance the overly weak eddies at lower levels, with the higher-resolution models not necessarily better representing the eddies.

Eddy-mean flow interactions through the breaking of Rossby waves have been shown to be key for blocking onset and maintenance as they advect low-PV air towards the higher latitudes (Nakamura and Wallace, 1993; Pelly and Hoskins, 2003; Altenhoff et al., 2008; Tyrlis and Hoskins, 2008). The advection results in the formation of a ridge linked to an anticyclonic anomaly over Greenland. In addition, recent studies have shown that diabatic processes, such as the release of latent heat from rising air masses within extratropical cyclones, help amplify the ridge building and the formation and maintenance of blocking (Pfahl et al., 2015; Steinfeld and Pfahl, 2019). ~~Enhanced cyclonic~~ Cyclonic wave breaking on the poleward side of the North Atlantic jet (southwest of Greenland) precedes blocking over Greenland (Woollings et al., 2008; Michel and Rivière, 2011). During Greenland blocking, the North Atlantic jet is zonal and shifted southward compared to its climatological position (Woollings et al., 2008, 2010; Davini et al., 2014; Madonna et al., 2017). Kwon et al. (2018) analysed the daily jet variability in the Community Earth System Model version 1 Large Ensemble and documented an underestimation of Greenland blocking linked to the infrequent and non-persistent southward displacement of the North Atlantic eddy-driven jet. Similar results were found for other CMIP5 models. For example, Iqbal et al. (2018) showed that most models underestimate eddy-driven jet variability because of infrequent southward excursions of the North Atlantic jet.

While it is well documented that Greenland blocking frequency is underestimated in climate models, little is known about the representation of the key processes that lead to Greenland blocking. Therefore, the aim of the present study is to investigate the Greenland blocking frequency and pattern representation in climate models, as well as the dynamical processes leading to Greenland blocking, with a focus on RWB. We analyse five large ensembles ($\geq$100 members) of atmosphere-only (AMIP) simulations, from the Half-a-degree Additional warming, Prognosis and Projected Impacts (HAPPI) project (Mitchell et al., 2017). With this large ensemble, we can assess the uncertainty in the representation of blocking due to internal atmospheric variability and the models themselves (structural uncertainty) and thus better evaluate the significance of biases. Finally, we look at how the frequency and dynamics of Greenland blocking may change in a 2°C warmer world relative to the pre-industrial period.

2 Data and Methods

2.1 The HAPPI large ensemble

The HAPPI international project provided a large multi-model ensemble with the aim to investigate the climate impacts in weak warming scenarios (Mitchell et al., 2017). In this study, we are interested in the present decade which covers 2006-2015 and a future decade in which the global annual mean temperature is 2°C warmer than the pre-industrial level ~~. Five~~ ($\sim +1.2$°C compared to the present decade). This multi-model ensemble comprises five atmospheric general circulation models (AGCM) ~~were run~~ with between 100 and 501 ~~times~~ members for each period. For the present decade, the observed sea surface tempera-

tures (SST) and sea ice were used. The greenhouse gases concentrations, aerosols, ozone, land use and land cover representative of 2006-2015 were held constant during the simulations. For the future decade, the CMIP5 ensemble mean SST and sea ice responses to global warming were added to the observed fields. More details about the simulations, models, and the forcings (atmospheric greenhouse gases, aerosols, ozone, and land) can be found in Mitchell et al. (2017) and Li et al. (2018). In the following, we use the daily outputs of geopotential at 500 hPa, zonal and meridional wind at 850 and 250 hPa from the five models CAM4-2degree, CanAM4, ECHAM6.3-LR, MIROC5, and NorESM1-HAPPI. The horizontal and vertical resolutions as well as the number of members for each model can be found in the Appendix (Table S1). The shortcomings of using a relatively short simulation period (10 years) to investigate climate variability is compensated by the large number of members available, which allows for robust statistics. Moreover, Davini and D'Andrea (2016) did not find substantial differences in blocking statistics from climate models when using ten years compared to longer periods.

2.2 Reanalysis

We utilize the ERA-Interim reanalysis (Dee et al., 2011) from the European Centre for Medium-Range Weather Forecasts as a reference. Six-hourly data are averaged to produce daily means and interpolated horizontally to a $0.5° \times 0.5°$ grid. We consider the nine winter (December-January-February, DJF) seasons during the 2006-2015 decade (starting in December 2006 and ending in February 2015), which correspond to the decade used for the HAPPI simulations (see Sec. 2.1). We use the zonal and meridional components of the wind at lower (850 hPa) and upper (250 hPa) tropospheric levels, the geopotential height at 500 hPa, and the absolute vorticity at 250 hPa. In the remainder of the text, we use the time-mean 850 hPa zonal winds as a proxy for the eddy-driven jet. As the North Atlantic jet is predominantly eddy-driven (Eichelberger and Hartmann, 2007; Woollings et al., 2010; Li and Wettstein, 2012), we expect similar results if we use 250 hPa winds instead.

2.3 Blocking detection

Blocking refers to quasi-stationary and persistent weather systems that obstruct the westerly flow. There are many ways to identify blocking using anomalies or meridional gradients of various fields, such as 500-hPa geopotential, potential vorticity or temperature (e.g. Tibaldi and Molteni, 1990; Pelly and Hoskins, 2003; Scherrer et al., 2006; Davini et al., 2012; Masato et al., 2012; Dunn-Sigouin and Son, 2013), and each method has its own shortcomings (Tyrlis et al., 2020). In this study, we use reversals in the meridional gradient of the geopotential height at 500 hPa (Z500) to identify blocks (Tibaldi and Molteni, 1990). We follow the criteria of Scherrer et al. (2006) and detect blocking, lasting for at least 5 days, by looking for Z500 meridional gradient reversals in 30° latitudinal bands (±15°) around every latitude between 35 and 75°N. ~~Blocking events~~ Blocked grid points are identified from daily data for both ERA-Interim and the HAPPI simulations using the models' original grids and the whole decade. An interpolation to a common grid before identifying blocking does not lead to substantial changes in the results (see Fig. S1 for NorESM1-HAPPI). ~~Blocking~~ Winter-time blocking climatologies are obtained by averaging all blocked ~~gridpoints over time and~~ grid points over time (excluding January, February 2006 and December 2015 to only keep full DJF seasons) and are expressed as a ~~fraction of time (in %~~percentage of the number of winter days (90×9=810 days). Greenland blocking days are defined when at least 10% of the area within 65-25°W/60-75°N (black box in Fig. 1f) is blocked.

Although 10% was subjectively chosen, it appears to capture relevant Greenland blocking days. The numbers of blocked days for each of the nine winters within the decade are averaged to give the mean DJF Greenland blocking frequency for each member. Composites of Greenland blocking are computed by averaging all days that exhibit blocking over Greenland.

2.4 Rossby wave breaking detection

Rossby wave breaking ~~occur~~ occurs when the waves elongate in a certain direction, break and dissipate. Anticyclonic wave breaking (AWB) occurs when the wave elongates along a northeast-southwest axis, typically on the equatorward flank of the jet, and acts to shift the eddy-driven jet poleward. Cyclonic wave breaking (CWB) occurs when the wave elongates along a northwest-southeast axis on the poleward flank of the jet to shift the eddy-driven jet equatorward. Here, we use the same detection algorithm as in Michel and Rivière (2011) based on the method of Rivière (2009) applied to the daily absolute vorticity fields interpolated on a regular $4.5° \times 4.5°$ spatial grid to capture the large-scale contour overturnings. The method identifies Rossby wave breaking via meridional reversals of absolute vorticity contours at 250 hPa. This method is known to provide similar statistics to those which use potential vorticity on different isentropic levels (Michel and Rivière, 2011; Barnes and Hartmann, 2012). This algorithm distinguishes between CWB and AWB by the direction of the contour reversal. Wave breaking frequencies are then derived by appropriately averaging over the binary mask fields. As CWB occurs mainly upstream of blocks (Altenhoff et al., 2008; Spensberger and Spengler, 2014), we define a separate target region for a CWB index (70°W-30°W/50°N-70°N) that is slightly equatorward and upstream of the target box used for the blocking index. This region corresponds to the largest CWB frequency when Greenland blocking occurs ~~(see e.g., Michel and Rivière, 2011, and the GB composites in Fig. 5~~ (see e.g., Michel and Rivière, 2011, and the Greenland blocking composites in Fig. 5d,e,f).

2.5 Anticyclone detection

We detect anticyclones using the method from Wernli and Schwierz (2006), which identifies the area covered by anticyclones using the outermost closed contour around a maximum in sea-level pressure. This procedure leads to problems over high topography, because the extrapolated sea-level pressure is very sensitive to near-surface temperatures. For this reason high topography is masked in many detection schemes for cyclones and anticyclones (c.f. intercomparsion in Neu et al., 2013).

As we are interested in anticyclones over Greenland, we thus adapt the procedure to use anomalies of 500-hPa geopotential with respect to the seasonal climatology as input to the anticyclone detection. Although about 200 hPa above Greenland's highest point, the 500-hPa level is the lowest level not intersecting the Greenland topography that is available for all models. We require a minimum height difference between the geopotential maximum and the outermost closed contour of 25 m (compared to 2 hPa in the original definition of the algorithm in Sprenger et al., 2017) and require a size of the anticyclone between 1 and 18 10^6 km^2 (consistent with the original definition in Sprenger et al., 2017).

We use this objective detection algorithm because even though a blocking can be considered as a stationary anticyclone, an anticyclone can occur without reversal of geopotential contours, which is the method used in this study to detect blocking. Thus, we are able to see if there are anticyclones over Greenland that are not linked to an overturning of a geopotential contour and without any minimum persistence.

2.6 ~~Significance of biases~~Statistical significance

2.6.1 For biases

The significance of biases is assessed with a two-sided t-test at a significance level of 90%. For the models, the 9-winter climatology is first computed for each member, then the ensemble mean and standard deviation are computed. Nine winters might be considered too short to accurately assess the blocking frequency due to its large interannual variability. However, using ERA-Interim, we show that none of the 30 climatologies of 9 consecutive winters (i.e. 1980-1989, 1981-1990, etc.) of blocking frequency is significantly different from the total 40-year (1979-2018) climatology (Fig. S2). ~~Therefore, to~~ To test the significance of biases, we compare the model mean to the observed 2006-2015 mean using an estimate of the variability from the standard deviation of 100 means of nine winters randomly chosen (with replacement) and non consecutive taken from the ~~30 consecutive 9-year winter means covering the~~ whole ERA-Interim period (~~1980-2018).~~ 1979-2018).

2.6.2 For composites

The significance of the composites was performed using a bootstrap method. For each member, X random winter days are averaged together, X being the number of days corresponding to the number of blocked days (for Figs. 5 and 7) or to the number of days with CWB index above the 95th percentile (for Fig. 6). We take the ensemble mean and repeat this operation 1000 times. Finally, the percentile at which the composite value is located in the bootstrapped distribution is found and all grid points with percentiles below the 10th and above the 90th percentiles are considered as significant.

3 Models biases

This section documents the biases in the HAPPI models (the ensemble means) with respect to the ERA-Interim reanalysis. A comprehensive characterization of the atmospheric mean state bias in the HAPPI models was performed by Li et al. (2018), so we hereafter summarize the main results of that work relevant to the current study and complement them with an analysis of the biases in blocking and RWB frequencies.

3.1 Blocking bias

Like most CMIP5 models (Anstey et al., 2013; Dunn-Sigouin and Son, 2013; Masato et al., 2013), the HAPPI models generally have too few blocks over the North Atlantic during winter (Fig. 1, blue shading). In the North Atlantic sector, blocking occurs in a few preferred regions ~~(Dole and Gordon, 1983; Lupo and Smith, 1995; Treidl et al., 1981)~~ (Treidl et al., 1981; Dole and Gordon, 1983; Lupo and Smith, 1995). The maximum in the subtropics (Fig. 1f) is a manifestation of the semi-permanent Azores High rather than a high frequency of blocking events (Davini et al., 2014). A second blocking region ($\sim$ 8-9%) is found over north-western Europe and a third over Greenland ($\sim$ 5-6%, black box). All ~~the~~ models underestimate blocking in the North Atlantic sector, with some models (e.g. CAM4-2degree) showing almost no blocking at all (i.e. a negative bias as large in magnitude as the climatology). ~~Most of the negative biases are~~ All models exhibit significant

(non-dotted) ~~, but this is not the case for~~ negative biases over Greenland and UK, with MIROC5 ~~, which~~ having also a significant positive bias southwest of Greenland. MIROC5 is the model with the smallest bias ~~overall, in particular~~ and ECHAM6.3-LR the model with the second lowest bias over Greenland. This is also obvious from Table 1 as ECHAM6.3-LR and MIROC5 are the models with the highest ensemble mean blocking frequencies and the only models where blocking occurs in all ensemble members.

Accurate Greenland blocking can occasionally be reproduced by a few members of some models even though these models exhibit ~~strong~~ negative biases in the ensemble mean. This highlights the advantage of using a large number of ensemble members (or long simulations) to sample relatively rare events such as blocking. Figure 2 shows the distributions of the nine-winter mean frequencies of Greenland blocking for each model (colored bars) and the lowest and highest blocking frequencies (dashed vertical lines for 5.6 and 14.1%) from the 31 mean DJF frequencies obtained for every possible decade (1979-1988, 1980-1989, etc) covering the ERA-Interim period (1979-2018). Three models of the HAPPI ensemble, CanAM4, NorESM1-HAPPI, and CAM4-2degree, have much lower blocking frequencies than ERA-Interim and only 9%, 6% and 2% of their distributions fall within ERA-Interim's range. These three models can on occasion simulate blocking with a frequency close to ERA-Interim's but they seem to lack an ingredient for blocking formation that can systematically increase the total blocking frequency in every member. Remarkably, more than half of CAM4-2degree's members have no blocking over Greenland (gray bar in Fig. 2a). ECHAM6.3-LR and MIROC5 perform better, with a fair number of members able to simulate ERA-Interim's blocking frequency for the decade 2006-2015 (12.68%, represented by the black solid line in Fig. 2). 74% of MIROC5 members and 47% of ECHAM6.3-LR members are within the full range of ERA-Interim (5.6-14.1%), with MIROC5's distribution overshooting ERA-Interim's and ECHAM6.3-LR's distribution undershooting ERA-Interim's. Our result for MIROC5 is in agreement with Masato et al. (2013) who showed that the CMIP5 coupled version of MIROC5 has a tendency to overestimate the GB frequency and to shift it over the Labrador Sea. Overall, MIROC5 is the model with the closest ensemble mean GB frequency to ERA-Interim.~~These results are in agreement with the areas of significant and non-significant biases shown in Fig. 1.~~

3.2 Large-scale atmospheric circulation biases

Similar to the CMIP5 ensemble mean, the majority of the HAPPI models exhibit a too zonal and too strong North Atlantic eddy-driven jet in winter (as illustrated by the positive bias in the low-level zonal wind in Fig. S3), with the exception of MIROC5 whose eddy-driven jet is too weak. ECHAM6.3-LR best reproduces the DJF climatological low-level zonal winds. All models underestimate the southwest-northeast tilt of the North Atlantic low-level jet, with ECHAM6.3-LR and CanAM4 having the most realistic North Atlantic tilt (not shown).

As blocking is detected from Z500, any bias in the mean state and variability of this field can influence the representation of blocking. The mean state bias is characterized by a trough that is not deep enough over eastern North America (60°W) and a ridge not pronounced enough over western Europe in most models (Fig. S4). This is in accordance with the biases in stationary waves, defined by the 500-hPa geopotential deviation from the zonal mean, exhibiting a weakened ridge consistent with the too zonal climatological jet, in four out of the five models (Fig. S5). MIROC5's Z500 mean state bias exhibits a meridional

dipole of opposite sign compared to the other models with a positive bias north of 50°N and a negative bias south of 50°N, respectively (Fig. S4d). ECHAM6.3-LR is also slightly different and shows only a slight negative bias close to Newfoundland at 50°N (Fig. S4c). This means that the trough at 60°W is too pronounced in ECHAM6.3-LR and not pronounced enough in MIROC5 in association with a too strong and too weak meridional gradient of Z500, respectively. MIROC5 is the model with the widest ridge, which extends too much to the west (Fig. S5d).

Biases in the mean state of the atmosphere could result from biases in the simulated variability (e.g. Kidston and Gerber, 2010; Kwon et al., 2018). For example, if Greenland blocking is too frequent with the jet too often shifted southward, we expect a southern bias in the mean wind state. Here, we examine the zonal wind variability by computing the standard deviation of the daily zonal wind at 850 hPa for each ensemble member separately before averaging over all members (Fig. 3). Similar results are observed for the wind at 250 hPa (not shown). In the reanalysis, the highest variability of the daily zonal wind (i.e. the highest standard deviations) in the North Atlantic is co-located with the climatological jet stream end and extends eastwards of 60°W over a broad latitudinal range ($\sim$ 40°-70°N, Fig. 3). ~~Similar~~ All HAPPI models exhibit standard deviation values ~~are found in all HAPPI models~~similar to ERA-Interim, however, only on the poleward side of the climatological jet between the southern tip of Greenland and Iceland. This suggests that the simulated North Atlantic daily jet is too infrequently in a southward-shifted position, similar to the results found in Kwon et al. (2018). MIROC5 and ECHAM6.3-LR are the models with the largest variability on the equatorward side of the mean jet ~~and the smallest mean-state biases with respect to~~ (30°N, Fig. S6) hence the smallest bias in wind variability.

3.3 Rossby wave breaking bias

RWB has been shown to play an important role for blocking and the formation and maintenance of weather regimes (e.g. Swenson and Straus, 2017). ~~Climatologies show~~ The ERA-Interim climatology of RWB frequency shows that AWB is ~~more frequent and located~~ most frequent on the equatorward side of the ~~jet at both low and upper levels (solid contours~~ mean jet (compare red contours to gray shading in Fig. ~~4 left) ,~~ S7f) while CWB is less frequent ~~and occurs~~ than AWB but shows a maximum frequency on the poleward side of the ~~jet (dashed contours~~ mean jet (compare blue contours to gray shading in Fig. ~~4 right) (Martius et al., 2007)~~S7f) (see also Martius et al., 2007). However, both types of RWB are generally more frequent than blocking. Since blocking formation often involves RWB (Altenhoff et al., 2008; Michel and Rivière, 2011; Masato et al., 2012; Spensberger and Spengler, 2014; Woollings et al., 2018), it is important to know how climate models represent RWB.

Most HAPPI models show a similar RWB pattern as ERA-Interim (Fig. S7), with the largest frequencies over the ocean, but their absolute values are generally too low (negative bias with blue shading in Fig. 4). Such negative biases in both AWB and CWB were also found for previous models versions (e.g., ECHAM5-HAM T63 in Béguin et al., 2013) using a different approach to detect wave breaking. MIROC5 stands out with in general too little AWB where ERA-Interim has a frequency maximum (blue shading superimposed to the grey contours in Fig. 4d right) and too much AWB to the north of this maximum (red shading in Fig. 4d left). MIROC5 is the model with the strongest negative biases in CWB (blue shading in Fig. 4 right). Overall, ECHAM6.3-LR is the model exhibiting the smallest biases in both AWB and CWB. The bias in CWB is also obvious in Table 1 with MIROC5 having the weakest mean CWB index and ECHAM6.3-LR the largest.

Table 1. ~~Number~~ For all models and experiments, this table provides the number of members which have at least one day with Greenland blocking, as defined by the 10% threshold of the blocking index, out of the total number of members~~and~~ , the mean wintertime blocking frequency over those selected members~~for both the Present~~ , and ~~Future experiments. The last column gives~~ the ~~whole~~ ensemble mean wintertime blocking frequency taking into account ~~the~~ all members ~~with no blocking~~ (as in Fig. 2). If all members exhibit blocked days, the mean blocking frequency (4th column) equals the full ensemble mean blocking frequency (5th column). The last ~~line corresponds to ERA-Interim~~ column gives the (~~2006-2015 as for~~ ensemble) wintertime mean of the ~~HAPPI models~~CWB index (all winter days are taken into account) in % of the box area as defined in Section 2.4. A value of 100% would mean that every grid point in the box exhibits CWB.

Model/Reanalysis	Experiment	#members	Blocking frequency (blocking members)	Blocking frequency (all members)	(Ens.) mean CWB index
CAM4-2degree	Present	213/501	1.75%	0.74%	7.6%
CanAM4	Present	97/100	2.88%	2.79%	10.1%
ECHAM6.3-LR	Present	100/100	5.69%	5.69%	11.6%
MIROC5	Present	100/100	12.47%	12.47%	4.7%
NorESM1-HAPPI	Present	119/125	2.54%	2.42%	8.4%
CAM4-2degree	Future	199/501	1.48%	0.59%	7.4%
CanAM4	Future	95/100	2.97%	2.82%	10.4%
ECHAM6.3-LR	Future	100/100	4.76%	4.76%	11.5%
MIROC5	Future	100/100	9.90%	9.90%	4.7%
NorESM1-HAPPI	Future	121/125	2.21%	2.14%	8.2%
ERA-Interim	2006-2015	1/1	12.68%	-	11.1%

4 Dynamics of Greenland blocking

As seen in the above description of the bias in the HAPPI models, ECHAM6.3-LR and MIROC5 are noticeably different from the other three models. These two models best reproduce the Greenland blocking climatology seen in ERA-Interim despite contrasting biases in the atmospheric mean state (Z500, U850, RWB) and variability (Z500, U850) over the North Atlantic. The models' differences are most obvious southwest of Greenland where MIROC5 shows positive bias in AWB frequency, Z500, stationary wave and a negative bias in CWB frequency and U850 while ECHAM6.3-LR shows the opposite bias sign or negligible bias. Table 1 summarizes the different behaviour of MIROC5 and ECHAM6.3-LR: MIROC5 has the largest mean blocking frequency and weakest mean CWB index whereas it is the opposite for ECHAM6.3-LR. In the following, we will focus on these two models and compare the mechanisms leading to Greenland blocking.

4.1 Composites over blocked days

In agreement with ERA-Interim, ECHAM6.3-LR and MIROC5 exhibit an anticyclonic anomaly over Greenland and stronger westerly zonal wind to the south of the North Atlantic during blocked days (Fig. 5). However, MIROC5 does not exhibit an

enhanced CWB frequency south of Greenland, as seen in ECHAM6.3-LR and ERA-Interim (compare the composites in Fig. 5e with panels d and f). This is curious, as several studies have shown that one of the key drivers of Greenland blocking is an enhanced frequency of CWB (Woollings et al., 2008; Michel and Rivière, 2011; Swenson and Straus, 2017; Madonna et al., 2019), which, through convergence of meridional eddy momentum fluxes, acts to shift the jet equatorwards (Thorncroft et al., 1993; Rivière and Orlanski, 2007). Table 1 shows the number of members in each ensemble used in the composites over the blocked days. The zonal wind at 850 hPa is anomalously south and zonal from North America to the Mediterranean for both models and ERA-Interim (Fig. 5j-l). Since the method detecting geopotential contours reversal is used to identify blocking, all composites exhibit a pronounced ridge over Greenland with a cyclonic overturning over the Labrador Sea. However, the associated anticyclonic (positive) anomaly of geopotential is larger for ECHAM6.3-LR and ERA-Interim than for MIROC5 (Fig. 5a-c). Even though MIROC5 does not exhibit enhanced CWB south of Greenland compared to ECHAM6.3-LR and ERA-Interim (Fig. 5~~c-e~~d-f), the three of them show a slight positive anomaly of AWB frequency close to Iceland hinting at an Ω-shape of the blocking (Fig. 5g-i) however smoothed in the composite of geopotential height. In essence, the comparison between ERA-Interim, ECHAM6.3-LR and MIROC5 demonstrates that MIROC5 produces a realistic blocking frequency but for unclear reasons.

4.2 Discussion

Of the five models examined here, ECHAM6.3-LR is the least biased in terms of mean state, variability, and RWB, and ~~slightly underestimates~~ the Greenland blocking frequency ~~.~~ is only underestimated by 2-3% as seen on Fig. 1c. Only MIROC5 has more realistic Greenland blocking, although, as ~~discussed~~shown previously, it shows much larger biases in the other fields. In this section, we discuss the RWB biases, ~~the role of CWB on~~ how CWB modifies the atmospheric circulation, and explore potential reasons explaining the above results.

RWB can drive the eddy-driven jet position by accelerating/decelerating the wind in specific locations but the link between RWB biases and wind biases is not so simple. However, we note that models with a too strong zonal wind over northern Europe (CAM4-2degree, ~~CanAm4~~CanAM4, ECHAM6.3-LR and NorESM1-HAPPI in Figs. S3 and ~~S6~~S8) are associated with a positive bias in AWB over southern Europe (Fig. 4): there are too many AWB events forcing the jet too far northwards. ECHAM6.3-LR and ERA-Interim exhibit an anticyclonic reversal of the absolute vorticity isolines south of the jet (∼30°N) linked to the meridionally-confined maximum of AWB frequency. In contrast, for MIROC5, the meridionally wide area of AWB reflects a smooth isoline reversal in the absolute vorticity field (Fig. ~~S7d~~S9d). Moreover, the meridional gradient of absolute vorticity over the North Atlantic in MIROC5 is clearly very weak compared to ECHAM6.3-LR and ERA-Interim, especially over the western side of the ocean basin, because of the weak mean zonal wind and its meridional gradient (absolute vorticity depends on the vertical component of the wind curl). This negative bias in absolute vorticity in addition to the weak trough in the stationary wave pattern over the Labrador Sea could explain the absence of CWB in MIROC5 ~~(Figs. S7d and S5d, respectively, Barnes and Polvani, 2013)~~ (Figs. S9d and S5d, respectively, Barnes and Polvani, 2013) whereas some waves can propagate and break anticyclonically anywhere in the North Atlantic (Figs. 4d and ~~S8~~S7). Barnes and Hartmann (2011) found that a weak absolute vorticity gradient poleward of the jet inhibits CWB occurrence. Although it hampers

Table 2. Ensemble mean and spread (standard deviation over the members) of the number of days in each category for ECHAM6.3-LR and MIROC5 and total number of days in each category for ERA-Interim. Unit: days. The CWB/no CWB categories distinguish the days for which the spatially averaged CWB frequency, as defined in Section 2.4, is greater than 0 / equals 0. GB stands for Greenland Blocking. The GB/no GB categories distinguish the blocked days from the non-blocked days, as defined in Section 2.3. The sum of the number of days in the four categories for each model and ERA-Interim equals the total number of winter (DJF) days in the decade 2006-2015.

	ECHAM6.3-LR		MIROC5		ERA-Interim	
	CWB	no CWB	CWB	no CWB	CWB	no CWB
GB	36.2 ± 14.9	10.0 ± 6.0	51.2 ± 13.6	49.8 ± 15.2	77	26
no GB	431.9 ± 20.5	333.9 ± 22.6	323.4 ± 20.1	385.6 ± 24.4	406	303

CWB, the weak absolute vorticity gradient may also promote blocking formation if we assume that potential vorticity behaves similarly to the absolute vorticity~~(Luo et al., 2019).~~ . Luo et al. (2019) showed in an idealised set-up that, at high latitudes, a weak mean meridional gradient of potential vorticity, associated with weak mean wind, leads to reduced energy dispersion, enhanced nonlinearity, and more persistent eddy forcing, favouring long and intense blocking. Even though MIROC5 does not exhibit more intense or longer blocking than ECHAM6.3-LR, this mechanism could also trigger blocking thus enhancing its frequency.

Our results suggest that Greenland blocking in MIROC5 is not necessarily linked to CWB, but that CWB can nevertheless lead to a ridge over Greenland and a local enhancement of the zonal wind. Figure 6 shows composites of the days with a CWB index (defined in Sec. 2.4) larger than the 95th percentile for ECHAM6.3-LR, MIROC5, and ERA-Interim. We see that when there is CWB southwest of Greenland, there is a positive geopotential anomaly (Fig. 6a-c), which is only sometimes associated with blocking (Fig. 6~~l-n~~m-o). This could be due to the fact that not all CWB events trigger blocking and/or that CWB events mainly occur during blocking formation but are much less frequent during the mature stage of blocks. If we account for some time for the block to form, we observe a slight increase in blocking frequency 1-2 days after CWB occurrence (not shown). The same is true for ERA-Interim, therefore, the absence of CWB during Greenland blocking in MIROC5 (Fig. 5e) is not due to a timing issue. MIROC5 exhibits more frequent blocking events with only a slightly longer duration (Fig. ~~S9~~S10). Thus, the high Greenland blocking frequency in MIROC5 results mainly from more blocking events detected rather than a longer duration of these events.

Table 2 shows that Greenland blocking occurs as frequently with CWB (GB-CWB) as without CWB (GB-no CWB) for MIROC5 (51.2 versus 49.8 days), whereas for ECHAM6.3-LR and ERA-Interim Greenland blocking occurs most frequently with CWB (36.2 versus 10.0 days for ECHAM6.3-LR and 77 versus 26 days for ERA-Interim). This difference probably arises from the lack of CWB in MIROC5. Also, the composites of the 500-hPa geopotential for the category GB-no CWB exhibits a westward shift of the anticyclonic anomaly compared to the GB-CWB category (see first row in Figs. S11, S12 and S13). This may reflect the blocking at a later stage of its lifetime as recently shown by Drouard et al. (2021) for the blocking of

cyclonic type typical over Greenland. Whether or not CWB occurs during Greenland blocking, the low-level zonal wind is always stronger south over the North Atlantic (see columns (a) and (b) of the fourth row in Figs. S11, S12 and S13).

Both ECHAM6.3-LR and MIROC5 tend to overestimate the presence of anticyclones, defined in Sec. 2.5, over Greenland (Fig. ~~S10~~S14). It seems that, for MIROC5, a weak mean zonal wind associated with the biases in geopotential and absolute vorticity favours the presence of anticyclones (positive geopotential height anomalies) over Greenland, whether or not CWB occurs. To conclude, while in reanalysis and ECHAM6.3-LR, CWB seems an important ingredient for Greenland blocking, this mechanism is not equally present in MIROC5.

5 Future changes in Greenland blocking and RWB

After having analyzed the dynamics of GB in the HAPPI large ensemble, we are interested to see how future changes in blocking are linked to changes in its driver, namely CWB, in ECHAM6.3-LR where CWB are fairly simulated, and in MIROC5, the model with the best Greenland blocking frequency compared to ERA-Interim.

In agreement with previous studies using CMIP3, CMIP5~~experiments (e.g., Sillmann and Croci-Maspoli, 2009; Barnes et al., 2012; Mas~~, and CMIP6 experiments (e.g., Sillmann and Croci-Maspoli, 2009; Barnes et al., 2012; Masato et al., 2013; Woollings et al., 2018; Davini and D'Andrea, 2020), we note a ~~decrease in the~~ weak and non-significant decrease between the present and future experiments in the percentage of blocked days (see Table 1) and in the ensemble mean blocking frequency over Greenland, in particular for ECHAM6.3-LR (up to ~~-0.6%of the time~~-0.5%, Fig. S15c) and MIROC5 (up to ~~-1.4%of the time). The decrease is weak and not significant (not shown)~~ -1.5%, Fig. S15d). This decrease is weaker compared to the studies cited above (e.g., -2 to -4% over Greenland in the CMIP multi-model mean responses in Fig. 6a-c of Davini and D'Andrea, 2020) mainly because the HAPPI future experiments represent a very mitigated warming scenario with a global mean temperature increase of $+2°C$ relative to pre-industrial climate compared to the ~~+2.6 to 4.8~~3.2 to 5.4°C at the end of the 21st century for the Representative Concentration Pathway 8.5 of CMIP5 (IPCC, 2013). ~~The large~~ Previous studies showed that the decrease in Greenland blocking frequency seems linked to the poleward shift of the North Atlantic eddy-driven jet, as expected from the response to changes in baroclinicity, mainly at upper levels, due to global warming (Harvey et al., 2014; Shaw et al., 2016; Yin, 2005). However, even though some studies found decreasing trends in blocking frequencies (Sillmann and Croci-Maspoli, 2009; Masato et al., 2013; Matsueda and Endo, 2017; Woollings et al., 2018), such trends are often found to not be significant and to be very dependent on the metric and field used to detect blocking (Collins et al., 2019; Wachowicz et al., 2020). The composites over the blocked days for the future experiment are very similar ~~between the present and future experiments (~~to the composites for the present period (compare Fig. 7 to the left and middle columns of Fig. 5). The blocking index used in the present study is not affected by the increase in geopotential height due to global warming (Christidis and Stott, 2015) contrary to other Greenland blocking indices (Wachowicz et al., 2020).

Although ECHAM6.3-LR and MIROC5 predict decreased Greenland blocking, there is no obvious decrease in CWB or increase in AWB as it would be expected from previous studies. Global warming is expected to enhance the upper-tropospheric

baroclinicity (Harvey et al., 2014), which affects the nature of breaking of Rossby waves, leading to more AWB in an idealized zonally symmetric quasi-geostrophic model (Rivière, 2011). Barnes and Hartmann (2010) and Barnes and Polvani (2013) related the future decrease in blocking frequency to a northward shifted jet that hinders CWB on the poleward flank of the jet over the North Atlantic. In the very mitigated scenario of the HAPPI models, AWB become less frequent at almost all longitudes around 30°N over the oceanic basins of the Northern Hemisphere in winter (red dashed contours in Fig. ~~S11~~S16). Over the North Atlantic, ~~CWB do not seem to change much (very weak values and noisy field ; not shown~~the CWB frequency does not change (noisy field with amplitudes below first contour level) and AWB are less frequent for both ECHAM6.3-LR and MIROC5 despite the 850-hPa zonal wind responses being different (Fig. 8). For ECHAM6.3-LR, the zonal wind is accelerated where AWB is less frequent, west of 20°W and is accelerated between 50°N-60°N in relation with more AWB to its southeastern side (Fig. 8a). For MIROC5, the link between the zonal wind and RWB responses is not clear as the zonal wind is accelerated to the north at $\sim$ 60°N between 80°W-10°E despite the decrease in AWB especially over the western part of the oceanic basin (west of 30°W) (Fig. 8b). Therefore, in these two HAPPI models, the link between the changes in the Greenland blocking frequency and its driver is not obvious nor as expected from previous studies.

6 Conclusions

In this study, we examine the representation of Greenland blocking in large ensembles of climate models simulations as well as the role of CWB as a driver. As blocking is a relatively rare event ($\simeq$10-20% of the time in winter), large ensembles are required to ensure a sufficient number of events to be able to draw robust conclusions. In line with previous studies which analysed various climate models (e.g. the CMIP5 multi-model ensemble, Anstey et al., 2013; Dunn-Sigouin and Son, 2013), we find that Greenland blocking frequency is strongly underestimated in three out of the five HAPPI models used here. We see that the underestimation of GB frequency is linked to too little variability in the low-level zonal wind over the southern part of the North Atlantic, on the equatorward flank of the eddy-driven jet. This lack of variability is also apparent in the negative bias in CWB, the main driver of Greenland blocking identified in reanalyses, which acts to push the eddy-driven jet to the south and advect low potential vorticity air poleward. We focus on the two models that have a fair representation of Greenland blocking frequency: ECHAM6.3-LR exhibits the smallest bias in the mean state and only slightly underestimates Greenland blocking frequency ~~(not significant using a t-test)~~ for the reasons cited above (low variability in wind to the south and CWB not frequent enough), while MIROC5 has large biases in mean climate but is best at representing Greenland blocking frequency. MIROC5 produces more events, which on average last slightly longer than in the other models. However, the mechanisms leading to blocking in MIROC5 appear to be different to those in ECHAM6.3-LR and documented for reanalyses. This difference is most apparent in CWB occurrence, which is severely underestimated, and thus at odds with the accurate Greenland blocking frequency.

Rossby wave breaking patterns are quite well represented ~~for most models~~by most models, MIROC5 being the exception, but there is still a negative bias for both AWB and CWB almost everywhere in the European-North Atlantic domain and a positive bias of AWB over the Mediterranean. The link between RWB and Greenland blocking in ECHAM6.3-LR is similar

to ERA-Interim with large CWB frequency during GB events and some blocking events when CWB occur southwest of Greenland. However, the link between CWB and Greenland blocking in MIROC5 is not clear. Indeed, MIROC5 exhibits a strong negative bias in CWB over most of the Northern Hemisphere. Even though there is a reversal of the isohypses (lines of equal geopotential), the CWB frequency and the associated geopotential anomaly are very weak during blocking events but we show that MIROC5 can still produce blocking from CWB events. Therefore, the dynamical link between CWB and Greenland blocking is present but not the main ingredient in triggering Greenland blocking in MIROC5. There must then be another process in this model that favors the northwards advection of airmasses over Greenland.

In agreement with previous studies, ECHAM6.3-LR and MIROC5 both exhibit a decreased frequency of Greenland blocking in the future experiments. However, we find that the decrease is not significant and not clearly linked to a reduced frequency of CWB, as could have been expected from previous studies (e.g., Barnes and Hartmann, 2012). Moreover, Greenland blocking composites of the geopotential, zonal wind, and RWB for the future period are very similar to the composites for the present period.

Our study highlights that, in order to ~~improve and~~ evaluate blocking representation in climate models, we ~~must consider both~~ should not just consider biases in the mean state~~biases and dynamical drivers such as RWB~~. It is also important to evaluate the representation of the known mechanisms that lead to blocking, such as CWB, which is an indicator for the eddy-mean flow interaction. Davini et al. (2017) started to tackle this issue by studying the representation of eddies in one climate model with various spatial resolutions, finding that higher resolution simulations do not necessarily better represent eddies. ~~The~~ A better understanding of the biases sources in the mechanisms leading to blocking ~~formation and its maintenance thus remains an open question~~in climate models is crucial to reduce those biases and improve the prediction of future changes.

Author contributions. C. Michel and E. Madonna equally contributed to the study (analysis and writing). C. Spensberger contributed to the writing and performed the anticyclone detection analysis. C. Li and S. Outten contributed to the manuscript with comments and suggestions.

Competing interests. Camille Li is a member of the editorial board of the journal.

Acknowledgements. The authors are grateful to the three anonymous reviewers whose comments helped to improve the manuscript. This work was partly funded by the Bjerknes Centre for Climate Research in Bergen through the Fast Track Initiative granted to Clio Michel and the strategic project EMULATE to Erica Madonna. The authors thank the European Centre for Medium-range Weather Forecast for providing the ERA-Interim analyses and the HAPPI project for providing the very large ensembles of simulations. We are also grateful to ETH Zurich for sharing their blocking and anticyclone detection algorithms. We acknowledge the Norwegian e-infrastructure for research and education UNINETT Sigma2 (project NS9770K) and the Research Council of Norway (projects 295046 KeyCLIM and 275269 COLUMBIA).

References

Altenhoff, A. M., Martius, O., Croci-Maspoli, M., Schwierz, C., and Davies, H. C.: Linkage of atmospheric blocks and synoptic-scale Rossby waves: A climatological analysis, Tellus A, 60, 1053–1063, https://doi.org/10.1111/j.1600-0870.2008.00354.x, 2008.

Anstey, J. A., Davini, P., Gray, L. J., Woollings, T. J., Butchart, N., Cagnazzo, C., Christiansen, B., Hardiman, S. C., Osprey, S. M., and Yang, S.: Multi-model analysis of Northern Hemisphere winter blocking: Model biases and the role of resolution, J. Geophys. Res.-Atmos., 118, 3956–3971, https://doi.org/10.1002/jgrd.50231, 2013.

Barnes, E. A. and Hartmann, D. L.: Influence of eddy-driven jet latitude on North Atlantic jet persistence and blocking frequency in CMIP3 integrations, Geophys. Res. Lett., 37, https://doi.org/10.1029/2010GL045700, 2010.

Barnes, E. A. and Hartmann, D. L.: Rossby wave scales, propagation, and the variability of eddy-driven jets, J. Atmos. Sci., 68, 2893–2908, https://doi.org/10.1175/JAS-D-11-039.1, 2011.

Barnes, E. A. and Hartmann, D. L.: Detection of Rossby wave breaking and its response to shifts of the midlatitude jet with climate change, J. Geophys. Res. Atmos., 117, https://doi.org/10.1029/2012JD017469, 2012.

Barnes, E. A. and Polvani, L.: Response of the midlatitude jets, and of their variability, to increased greenhouse gases in the CMIP5 models, J. Climate, 26, 7117–7135, https://doi.org/10.1175/JCLI-D-12-00536.1, 2013.

Barnes, E. A., Slingo, J., and Woollings, T.: A methodology for the comparison of blocking climatologies across indices, models and climate scenarios, Climate Dyn., 38, 2467–2481, https://doi.org/10.1007/s00382-011-1243-6, 2012.

Béguin, A., Martius, O., Sprenger, M., Spichtinger, P., Folini, D., and Wernli, H.: Tropopause level Rossby wave breaking in the Northern Hemisphere: a feature-based validation of the ECHAM5-HAM climate model, Int. J. Climatol., 33, 3073–3082, https://doi.org/10.1002/joc.3631, 2013.

Berckmans, J., Woollings, T., Demory, M.-E., Vidale, P.-L., and Roberts, M.: Atmospheric blocking in a high resolution climate model: influences of mean state, orography and eddy forcing, Atmos. Sci. Lett., 14, 34–40, https://doi.org/10.1002/asl2.412, 2013.

Chen, X. and Luo, D.: Arctic sea ice decline and continental cold anomalies: Upstream and downstream effects of Greenland blocking, Geophys. Res. Lett., 44, 3411–3419, https://doi.org/10.1002/2016GL072387, 2017.

Christidis, N. and Stott, P. A.: Changes in the geopotential height at 500 hPa under the influence of external climatic forcings, Geophys. Res. Lett., 42, 10 798–10 806, https://doi.org/10.1002/2015GL066669, 2015.

Collins, M., Sutherland, M., Bouwer, L., Cheong, S.-M., Frölicher, T., Combes, H. J. D., Roxy, M. K., Losada, I., McInnes, K., Ratter, B., Rivera-Arriaga, E., Susanto, R., Swingedouw, D., and Tibig, L.: Extremes, Abrupt Changes and Managing Risk, vol. IPCC Special Report on the Ocean and Cryosphere in a Changing Climate, chap. 6, p. in press, 2019.

Davini, P. and D'Andrea, F.: Northern Hemisphere atmospheric blocking representation in global climate models: Twenty years of improvements?, J. Climate, 29, 8823–8840, https://doi.org/10.1175/JCLI-D-16-0242.1, 2016.

Davini, P. and D'Andrea, F.: From CMIP3 to CMIP6: Northern Hemisphere atmospheric blocking simulation in present and future climate, J. Climate, 33, 10 021–10 038, https://doi.org/10.1175/JCLI-D-19-0862.1, 2020.

Davini, P., Cagnazzo, C., Gualdi, S., and Navarra, A.: Bidimensional Diagnostics, Variability, and Trends of Northern Hemisphere Blocking, J. Climate, 25, 6496–6509, https://doi.org/10.1175/JCLI-D-12-00032.1, 2012.

Davini, P., Cagnazzo, C., Fogli, P. G., Manzini, E., Gualdi, S., and Navarra, A.: European blocking and Atlantic jet stream variability in the NCEP/NCAR reanalysis and the CMCC-CMS climate model, Climate Dyn., 43, 71–85, https://doi.org/10.1007/s00382-013-1873-y, 2014.

Davini, P., Corti, S., D'Andrea, F., Rivière, G., and von Hardenberg, J.: Improved winter European atmospheric blocking frequencies in high-resolution global climate simulations, J. Adv. Model. Earth Sy., 9, 2615–2634, https://doi.org/10.1002/2017MS001082, 2017.

Dee, D. P., Uppala, S., Simmons, A., Berrisford, P., Poli, P., Kobayashi, S., Andrae, U., Balmaseda, M., Balsamo, G., Bauer, d. P., et al.: The ERA-Interim reanalysis: Configuration and performance of the data assimilation system, Quart. J. Roy. Meteor. Soc., 137, 553–597, https://doi.org/10.1002/qj.828, 2011.

Dole, R. M. and Gordon, N. D.: Persistent anomalies of the extratropical Northern Hemisphere wintertime circulation: Geographical distribution and regional persistence characteristics, Mon. Wea. Rev., 111, 1567–1586, https://doi.org/10.1175/1520-0493(1983)111<1567:PAOTEN>2.0.CO;2, 1983.

Drouard, M., Woollings, T., Sexton, D. M. H., and McSweeney, C. F.: Dynamical differences between short and long blocks in the Northern Hemisphere, J. Geophys. Res. Atmos., 126, e2020JD034 082, https://doi.org/10.1029/2020JD034082, 2021.

Dunn-Sigouin, E. and Son, S.-W.: Northern Hemisphere blocking frequency and duration in the CMIP5 models, J. Geophys. Res. Atmos., 118, 1179–1188, https://doi.org/10.1002/jgrd.50143, 2013.

Eichelberger, S. J. and Hartmann, D. L.: Northern Hemisphere blocking frequency and duration in the CMIP5 models, J. Climate, 20, 5149–5163, https://doi.org/10.1175/JCLI4279.1, 2007.

Fettweis, X., Hanna, E., Lang, C., Belleflamme, A., Erpicum, M., and Gallée, H.: Important role of the mid-tropospheric atmospheric circulation in the recent surface melt increase over the Greenland ice sheet, The Cryosphere, 7, 241–248, https://doi.org/10.5194/tc-7-241-2013, 2013.

Hanna, E., Cappelen, J., Fettweis, X., Mernild, S. H., Mote, T. L., Mottram, R., Steffen, K., Ballinger, T. J., and Hall, R. J.: Greenland surface air temperature changes from 1981 to 2019 and implications for ice-sheet melt and mass-balance change, Int. J. Climatol., 41, E1336–E1352, https://doi.org/10.1002/joc.6771, 2021.

Harvey, B., Shaffrey, L., and Woollings, T.: Equator-to-pole temperature differences and the extra-tropical storm track responses of the CMIP5 climate models, Climate Dynamics, 43, 1171–1182, https://doi.org/10.1007/s00382-013-1883-9, 2014.

Harvey, B., Cook, P., Shaffrey, L., and Schiemann, R.: The Response of the Northern Hemisphere Storm Tracks and Jet Streams to Climate Change in the CMIP3, CMIP5, and CMIP6 Climate Models, J. Geophys. Res. Atmos., 125, https://doi.org/10.1029/2020JD032701, 2020.

Hermann, M., Papritz, L., and Wernli, H.: A Lagrangian analysis of the dynamical and thermodynamic drivers of large-scale Greenland melt events during 1979–2017, Weather and Climate Dynamics, 1, 497–518, https://doi.org/10.5194/wcd-1-497-2020, 2020.

IPCC: Summary for policymakers, vol. Climate Change 2013: The Physical Science Basis. Contribution of Working Group I to the Fifth Assessment Report of the Intergovernmental Panel on Climate Change, Cambridge University Press, Cambridge, United Kingdom and New York, NY, USA, 2013.

Iqbal, W., Leung, W.-N., and Hannachi, A.: Analysis of the variability of the North Atlantic eddy-driven jet stream in CMIP5, Climate Dyn., 51, 235–247, https://doi.org/10.1007/s00382-017-3917-1, 2018.

Kidston, J. and Gerber, E.: Intermodel variability of the poleward shift of the austral jet stream in the CMIP3 integrations linked to biases in 20th century climatology, Geophys. Res. Lett., 37, https://doi.org/10.1029/2010GL042873, 2010.

Kwon, Y.-O., Camacho, A., Martinez, C., and Seo, H.: North Atlantic winter eddy-driven jet and atmospheric blocking variability in the Community Earth System Model version 1 Large Ensemble simulations, Climate Dyn., 51, 3275–3289, https://doi.org/10.1007/s00382-018-4078-6, 2018.

Li, C. and Wettstein, J. J.: Thermally Driven and Eddy-Driven Jet Variability in Reanalysis, J. Climate, 25, 1587–1596, https://doi.org/10.1175/JCLI-D-11-00145.1, 2012.

Li, C., Michel, C., Graff, L. S., Bethke, I., Zappa, G., Bracegirdle, T. J., Fischer, E., Harvey, B. J., Iversen, T., King, M. P., et al.: Midlatitude atmospheric circulation responses under 1.5 and 2.0 degrees C warming and implications for regional impacts, Earth Syst. Dynam., 9, 359–382, https://doi.org/10.5194/esd-9-359-2018, 2018.

Luo, D., Zhang, W., Zhong, L., and Dai, A.: A nonlinear theory of atmospheric blocking: A potential vorticity gradient view, J. Atmos. Sci., 76, 2399–2427, https://doi.org/10.1175/JAS-D-18-0324.1, 2019.

Lupo, A. R. and Smith, P. J.: Climatological features of blocking anticyclones in the Northern Hemisphere, Tellus A, 47, 439–456, https://doi.org/10.1034/j.1600-0870.1995.t01-3-00004.x, 1995.

Madonna, E., Li, C., Grams, C. M., and Woollings, T.: The link between eddy-driven jet variability and weather regimes in the North Atlantic-European sector, Quart. J. Roy. Meteor. Soc., 143, 2960–2972, https://doi.org/10.1002/qj.3155, 2017.

Madonna, E., Li, C., and Wettstein, J. J.: Suppressed eddy driving during southward excursions of the North Atlantic jet on synoptic to seasonal time scales, Atmos. Sci. Lett., 20, e937, https://doi.org/10.1002/asl.937, 2019.

Martius, O., Schwierz, C., and Davies, H. C.: Breaking Waves at the Tropopause in the Wintertime Northern Hemisphere: Climatological Analyses of the Orientation and the Theoretical LC1/2 Classification, J. Atmos. Sci., 64, 2576–2592, https://doi.org/10.1175/JAS3977.1, 2007.

Masato, G., Hoskins, B., and Woollings, T. J.: Wave-breaking characteristics of midlatitude blocking, Quart. J. Roy. Meteor. Soc., 138, 1285–1296, https://doi.org/10.1002/qj.990, 2012.

Masato, G., Hoskins, B. J., and Woollings, T.: Winter and summer Northern Hemisphere blocking in CMIP5 models, J. Climate, 26, 7044–7059, https://doi.org/10.1175/JCLI-D-12-00466.1, 2013.

Matsueda, M. and Endo, H.: The robustness of future changes in Northern Hemisphere blocking: A large ensemble projection with multiple sea surface temperature patterns, Geophys. Res. Lett., 44, 5158–5166, https://doi.org/10.1002/2017GL073336, 2017.

McLeod, J. T. and Mote, T. L.: Assessing the role of precursor cyclones on the formation of extreme Greenland blocking episodes and their impact on summer melting across the Greenland ice sheet, J. Geophys. Res.-Atmos., 120, 12 357—-12 377, https://doi.org/10.1002/2015JD023945, 2015.

Michel, C. and Rivière, G.: The link between Rossby wave breakings and weather regime transitions, J. Atmos. Sci., 68, 1730–1748, https://doi.org/10.1175/2011JAS3635.1, 2011.

Mitchell, D., AchutaRao, K., Bethke, I., Beyerle, U., Ciavarella, A., Forster, P., Fuglestvedt, J., Gillett, N., Haustein, K., Ingram, W., et al.: Half a degree additional warming, prognosis and projected impacts (HAPPI): background and experimental design, Geosci. Model Dev., 10, 571–583, https://doi.org/10.5194/gmd-10-571-2017, 2017.

Nakamura, H. and Wallace, J. M.: Synoptic behavior of baroclinic eddies during the blocking onset, Mon. Wea. Rev., 121, 1892–1903, https://doi.org/10.1175/1520-0493(1993)121<1892:SBOBED>2.0.CO;2, 1993.

Neu, U., Akperov, M. G., Bellenbaum, N., Benestad, R., Blender, R., Caballero, R., Cocozza, A., Dacre, H. F., Feng, Y., Fraedrich, K., Grieger, J., Gulev, S., Hanley, J., Hewson, T., Inatsu, M., Keay, K., Kew, S. F., Kindem, I., Leckebusch, G. C., Liberato, M. L. R., Lionello, P., Mokhov, I. I., Pinto, J. G., Raible, C. C., Reale, M., Rudeva, I., Schuster, M., Simmonds, I., Sinclair, M., Sprenger, M., Tilinina, N. D., Trigo, I. F., Ulbrich, S., Ulbrich, U., Wang, X. L., and Wernli, H.: IMILAST: A Community Effort to Intercompare Extratropical Cyclone Detection and Tracking Algorithms, Bull. Amer. Meteor. Soc., 94, 529–547, https://doi.org/10.1175/bams-d-11-00154.1, 2013.

Pelly, J. L. and Hoskins, B. J.: A new perspective on blocking, J. Atmos. Sci., 60, 743–755, https://doi.org/10.1175/1520-0469(2003)060<0743:ANPOB>2.0.CO;2, 2003.

Pfahl, S. and Wernli, H.: Quantifying the relevance of atmospheric blocking for co-located temperature extremes in the Northern Hemisphere on (sub-)daily time scales, Geophys. Res. Lett., 39, https://doi.org/10.1029/2012GL052261, 2012.

Pfahl, S., Schwierz, C., Croci-Maspoli, M., Grams, C. M., and Wernli, H.: Importance of latent heat release in ascending air streams for atmospheric blocking, Nature Geoscience, 8, 610–614, https://doi.org/10.1038/ngeo2487, 2015.

Pithan, F., Shepherd, T. G., Zappa, G., and Sandu, I.: Climate model biases in jet streams, blocking and storm tracks resulting from missing orographic drag, Geophys. Res. Lett., 43, 7231–7240, https://doi.org/10.1002/2016GL069551, 2016.

Rex, D. F.: Blocking action in the middle troposphere and its effect upon regional climate, Tellus, 2, 275–301, https://doi.org/10.1111/j.2153-3490.1950.tb00331.x, 1950.

Rivière, G.: Effect of latitudinal variations in low-level baroclinicity on eddy life cycles and upper-tropospheric wave-breaking processes, J. Atmos. Sci., 66, 1569–1592, https://doi.org/10.1175/2008JAS2919.1, 2009.

Rivière, G.: A dynamical interpretation of the poleward shift of the jet streams in global warming scenarios, J. Atmos. Sci., 68, 1253–1272, https://doi.org/10.1175/2011JAS3641.1, 2011.

Rivière, G. and Orlanski, I.: Characteristics of the Atlantic storm-track eddy activity and its relation with the North Atlantic Oscillation, J. Atmos. Sci., 64, 241–266, https://doi.org/10.1175/JAS3850.1, 2007.

Scaife, A. A., Woollings, T., Knight, J., Martin, G., and Hinton, T.: Atmospheric blocking and mean biases in climate models, J. Climate, 23, 6143–6152, https://doi.org/10.1175/2010JCLI3728.1, 2010.

Schaller, N., Sillmann, J., Anstey, J., Fischer, E. M., Grams, C. M., and Russo, S.: Influence of blocking on Northern European and Western Russian heatwaves in large climate model ensembles, Environ. Res. Lett., 13, 054 015, https://doi.org/10.1088/1748-9326/aaba55, 2018.

Scherrer, S. C., Croci-Maspoli, M., Schwierz, C., and Appenzeller, C.: Two–dimensional indices of atmospheric blocking and their statistical relationship with winter climate patterns in the Euro-Atlantic region, Int. J. Climatol., 26, 233–249, https://doi.org/10.1002/joc.1250, 2006.

Schiemann, R., Demory, M.-E., Shaffrey, L. C., Strachan, J., Vidale, P. L., Mizielinski, M. S., Roberts, M. J., Matsueda, M., Wehner, M. F., and Jung, T.: The resolution sensitivity of Northern Hemisphere blocking in four 25-km atmospheric global circulation models, J. Climate, 30, 337–358, https://doi.org/10.1175/JCLI-D-16-0100.1, 2017.

Schiemann, R., Athanasiadis, P., Barriopedro, D., Doblas-Reyes, F., Lohmann, K., Roberts, M. J., Sein, D. V., Roberts, C. D., Terray, L., and Vidale, P. L.: Northern Hemisphere blocking simulation in current climate models: evaluating progress from the Climate Model Intercomparison Project Phase 5 to 6 and sensitivity to resolution, Weather and Climate Dynamics, 1, 277–292, https://doi.org/10.5194/wcd-1-277-2020, 2020.

Shaw, T., Baldwin, M., Barnes, E. A., Caballero, R., Garfinkel, C., Hwang, Y.-T., Li, C., O'Gorman, P., Rivière, G., Simpson, I., et al.: Storm track processes and the opposing influences of climate change, Nature Geoscience, 9, 656–664, https://doi.org/10.1038/ngeo2783, 2016.

Sillmann, J. and Croci-Maspoli, M.: Present and future atmospheric blocking and its impact on European mean and extreme climate, Geophys. Res. Lett., 36, https://doi.org/10.1029/2009GL038259, 2009.

Spensberger, C. and Spengler, T.: A New Look at Deformation as a Diagnostic for Large-Scale Flow, J. Atmos. Sci., 71, 4221–4234, https://doi.org/10.1175/JAS-D-14-0108.1, 2014.

Sprenger, M., Fragkoulidis, G., Binder, H., Croci-Maspoli, M., Graf, P., Grams, C. M., Knippertz, P., Madonna, E., Schemm, S., Škerlak, B., and Wernli, H.: Global Climatologies of Eulerian and Lagrangian Flow Features based on ERA-Interim, Bull. Amer. Meteor. Soc., 98, 1739–1748, https://doi.org/10.1175/BAMS-D-15-00299.1, 2017.

Steinfeld, D. and Pfahl, S.: The role of latent heating in atmospheric blocking dynamics: a global climatology, Climate Dyn., 53, 6159–6180, https://doi.org/10.1007/s00382-019-04919-6, 2019.

Swenson, E. T. and Straus, D. M.: Rossby wave breaking and transient eddy forcing during Euro-Atlantic circulation regimes, J. Atmos. Sci., 74, 1735–1755, https://doi.org/10.1175/JAS-D-16-0263.1, 2017.

Thorncroft, C., Hoskins, B., and McIntyre, M.: Two paradigms of baroclinic-wave life-cycle behaviour, Quart. J. Roy. Meteor. Soc., 119, 17–55, https://doi.org/10.1002/qj.49711950903, 1993.

Tibaldi, S. and Molteni, F.: On the operational predictability of blocking, Tellus A, 42, 343–365, https://doi.org/10.1034/j.1600-0870.1990.t01-2-00003.x, 1990.

Treidl, R., Birch, E., and Sajecki, P.: Blocking action in the Northern Hemisphere: A climatological study, Atmosphere-ocean, 19, 1–23, https://doi.org/10.1080/07055900.1981.9649096, 1981.

Trigo, R., Trigo, I., DaCamara, C., and Osborn, T.: Climate impact of the European winter blocking episodes from the NCEP/NCAR Reanalyses, Climate Dyn., 23, 17–28, https://doi.org/10.1007/s00382-004-0410-4, 2004.

Tyrlis, E. and Hoskins, B.: The morphology of Northern Hemisphere blocking, J. Atmos. Sci., 65, 1653–1665, https://doi.org/10.1175/2007JAS2338.1, 2008.

Tyrlis, E., Bader, J., Manzini, E., and Matei, D.: Reconciling different methods of high-latitude blocking detection, Quart. J. Roy. Meteor. Soc., pp. 1–27, https://doi.org/10.1002/qj.3960, 2020.

Van den Broeke, M. R., Enderlin, E. M., Howat, I. M., Kuipers Munneke, P., Noël, B. P., Jan Van De Berg, W., Van Meijgaard, E., and Wouters, B.: On the recent contribution of the Greenland ice sheet to sea level change, The Cryosphere, 10, 1933–1946, https://doi.org/10.5194/tc-10-1933-2016, 2016.

Vial, J. and Osborn, T. J.: Assessment of atmosphere-ocean general circulation model simulations of winter northern hemisphere atmospheric blocking, Climate Dyn., 39, 95–112, https://doi.org/10.1007/s00382-011-1177-z, 2012.

Wachowicz, L. J., Preece, J. R., Mote, T. L., Barrett, B. S., and Henderson, G. R.: Historical trends of seasonal Greenland blocking under different blocking metrics, Int. J. Climatol., 41, E3263–E32782 507, https://doi.org/10.1002/joc.6923, 2020.

Ward, J. L., Flanner, M. G., and Dunn-Sigouin, E.: Impacts of Greenland block location on clouds and surface energy fluxes over the Greenland Ice Sheet, J. Geophys. Res. Atmos., 125, e2020JD033 172, https://doi.org/10.1029/2020JD033172, 2020.

Wernli, H. and Schwierz, C.: Surface cyclones in the ERA40 dataset (1958- 2001). Part I: Novel identification method and global climatology, J. Atmos. Sci., 63, 2486–2507, https://doi.org/10.1175/JAS3766.1, 2006.

Woollings, T., Hoskins, B., Blackburn, M., and Berrisford, P.: A new Rossby wave–breaking interpretation of the North Atlantic Oscillation, J. Atmos. Sci., 65, 609–626, https://doi.org/10.1175/2007JAS2347.1, 2008.

Woollings, T., Hannachi, A., and Hoskins, B.: Variability of the North Atlantic eddy-driven jet stream, Quart. J. Roy. Meteor. Soc., 136, 856–868, https://doi.org/10.1002/qj.625, 2010.

Woollings, T., Barriopedro, D., Methven, J., Son, S.-W., Martius, O., Harvey, B., Sillmann, J., Lupo, A. R., and Seneviratne, S.: Blocking and its response to climate change, Curr. Clim. Change Rep., 4, 287–300, https://doi.org/10.1007/s40641-018-0108-z, 2018.

Yin, J. H.: A consistent poleward shift of the storm tracks in simulations of 21st century climate, Geophys. Res. Lett., 32, https://doi.org/10.1029/2005GL023684, 2005.

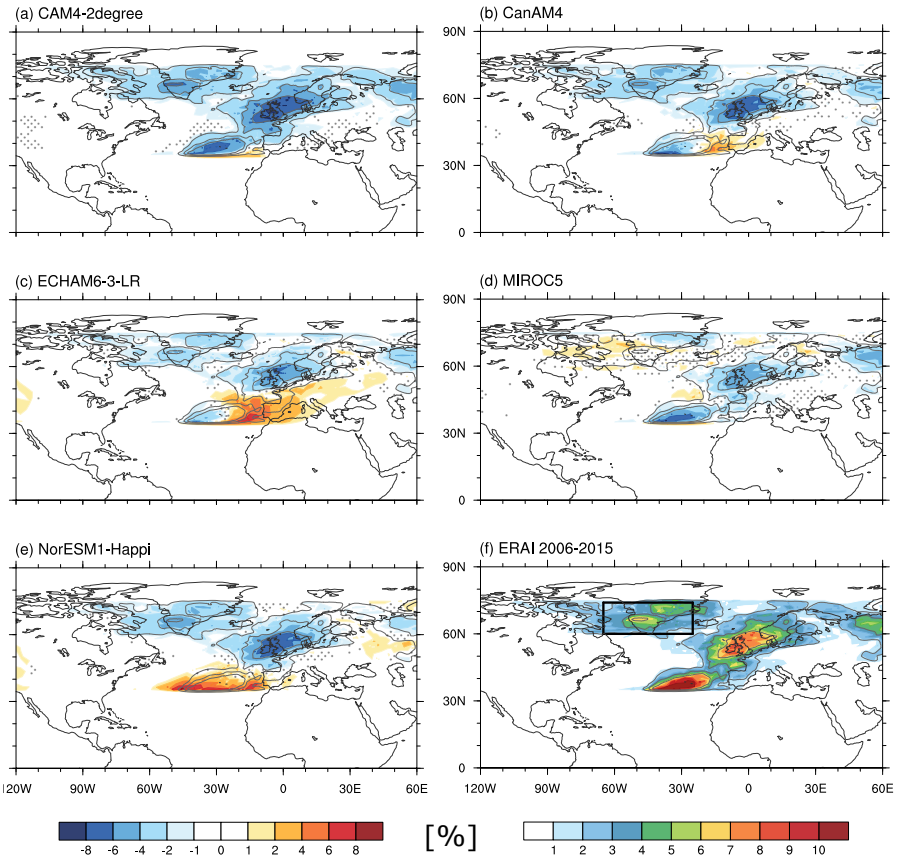

Figure 1. (a-e) Bias in winter (DJF) blocking frequency for the five models (ensemble mean of the blocking frequency –minus ERA-Interim) and (f) ERA-Interim DJF blocking climatology for 2006-2015 (in frequency, as %). ~~Black~~ Dark gray lines show the smoothed 2, 4 and 6% contours for ERA-Interim (2006-2015). The black box shows the main region of Greenland blocking in ERA-Interim. Biases that are not significant at the 90% level are dotted and there are no dots where there is no blocking.

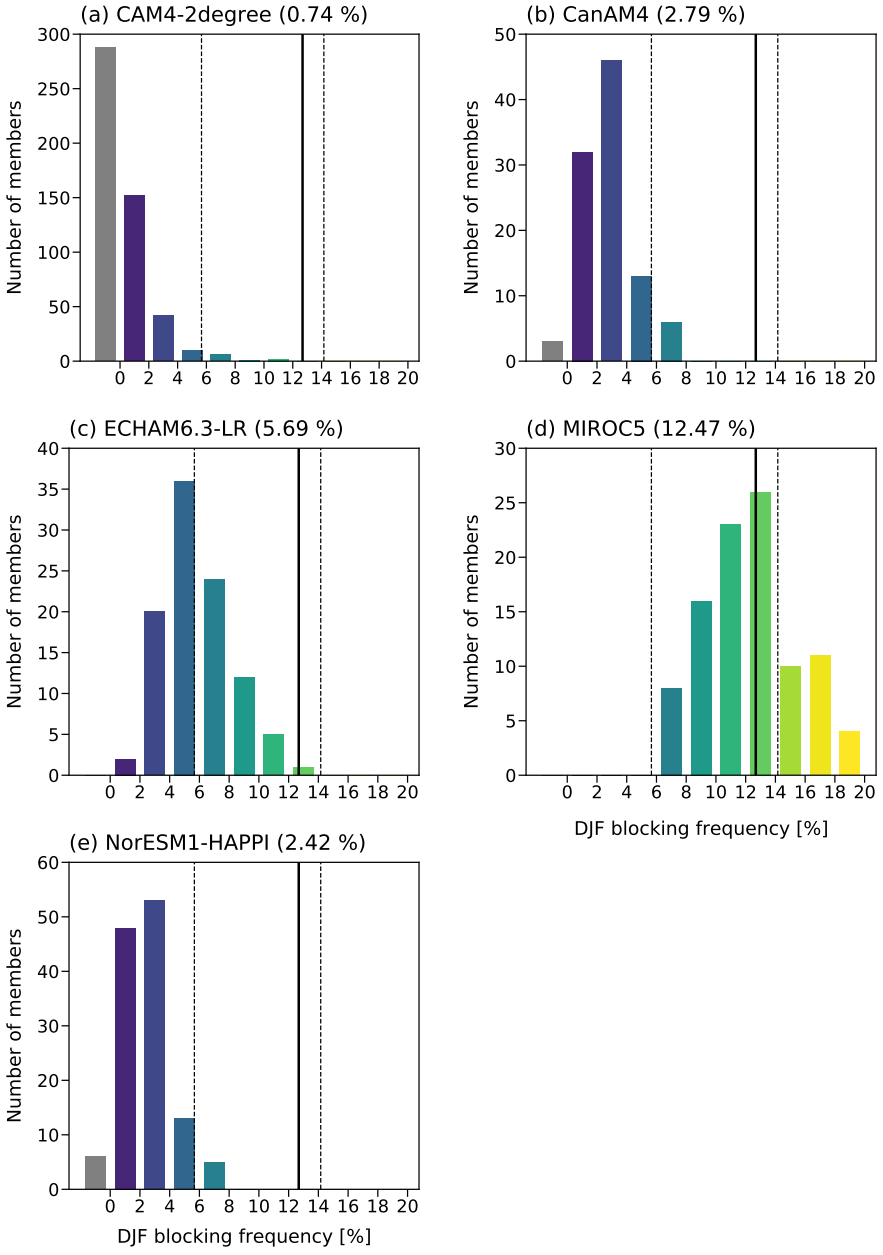

Figure 2. Distributions of the nine-winter (DJF) mean Greenland blocking frequency (in 2% bins) for each ensemble. The mean frequency of each model is shown in the title and given in Table 1. Shown in every panel ~~are~~ is the mean Greenland blocking frequency ~~in~~ from ERA-Interim for 2006-2015, which is 12.68% (black line), and the minimum/maximum ~~(5.66/14.16%)~~ blocking frequencies from nine-consecutive winters for the whole ERA-Interim ~~(~~period of 1979-2018, which are 5.66 and 14.16% respectively (dashed lines). Gray bars show the number of members with no GB blocking in the nine-year period.

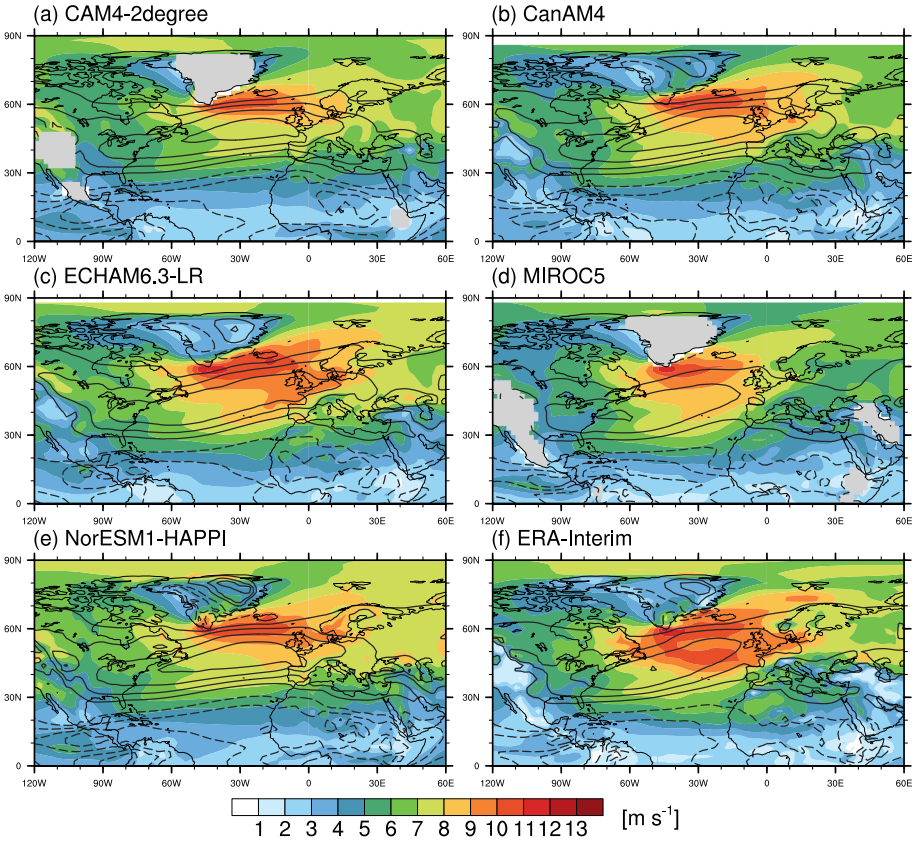

Figure 3. Ensemble means of the DJF mean daily standard deviation of the 850-hPa zonal wind ~~at 850 hPa~~ (shading, in m s^{-1}) and of the DJF 850-hPa zonal wind climatology (~~first contour and~~ contours, interval: 3 m s^{-1}, zero contour omitted~~and~~, negative values with dashed lines) for (a) CAM4-2degree, (b) CanAM4, (c) ECHAM6.3-LR, (d) MIROC5, and (e) NorESM1-HAPPI~~, and (f) ERA-Interim~~. The daily standard deviation is calculated for each member separately and then averaged over the ensemble. (f) DJF mean daily standard deviation (shading, in m s^{-1}) and climatology (contours, interval: 3 m s^{-1}, zero contour omitted, negative values with dashed lines) of the 850-hPa zonal wind for the period 2006-2015 of ERA-Interim.

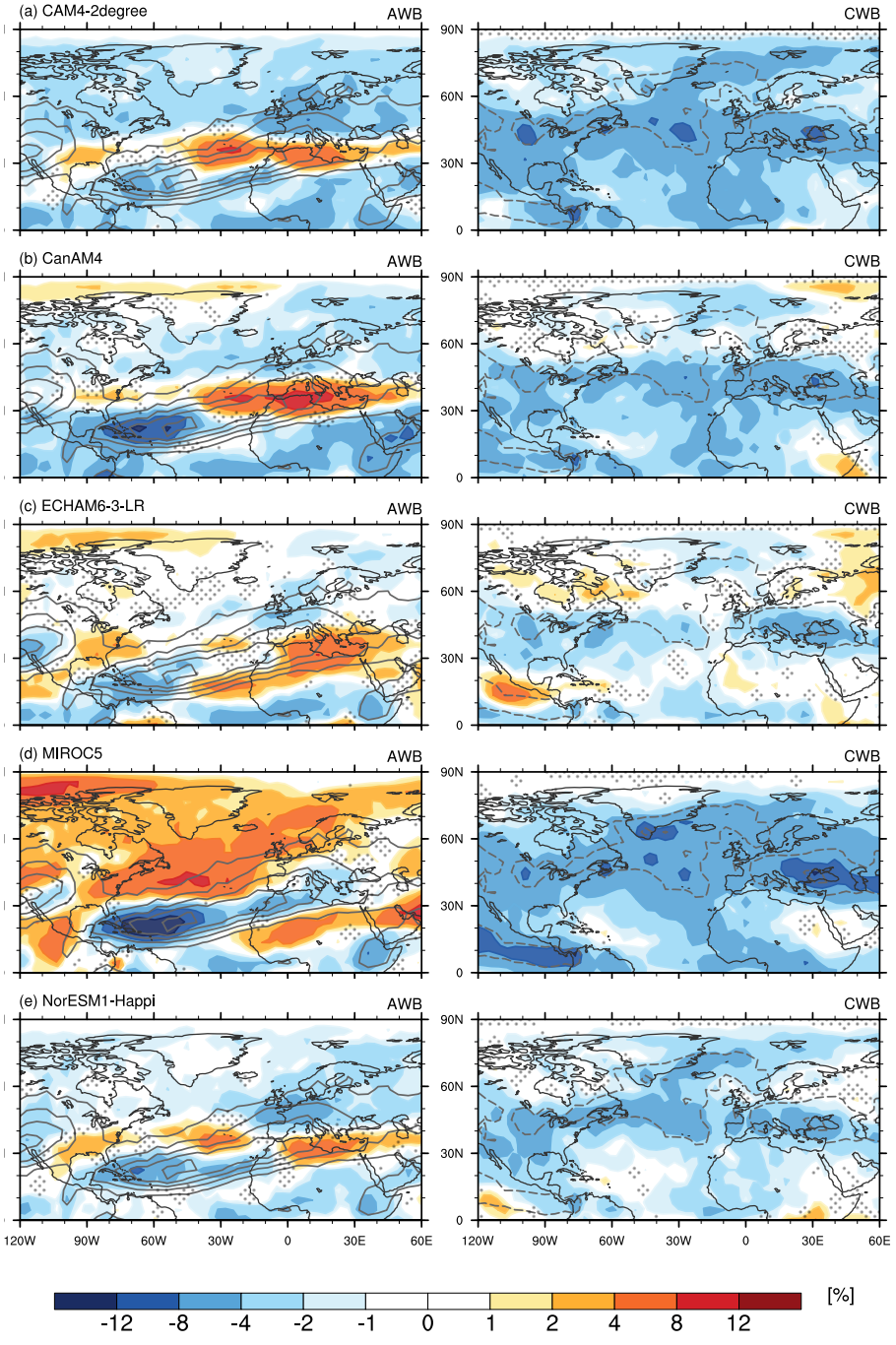

Figure 4. Bias in anticyclonic (AWB, left) and cyclonic (CWB, right) wave breaking for the five HAPPI models. Bias as shown as frequencies (in % of time), while the ERA-Interim climatology for the period 2006-2015 is shown in contours (starting at 10%, in 5% steps, left solid for AWB and right dashed for CWB). Black dots mark biases that are not statistically significant.

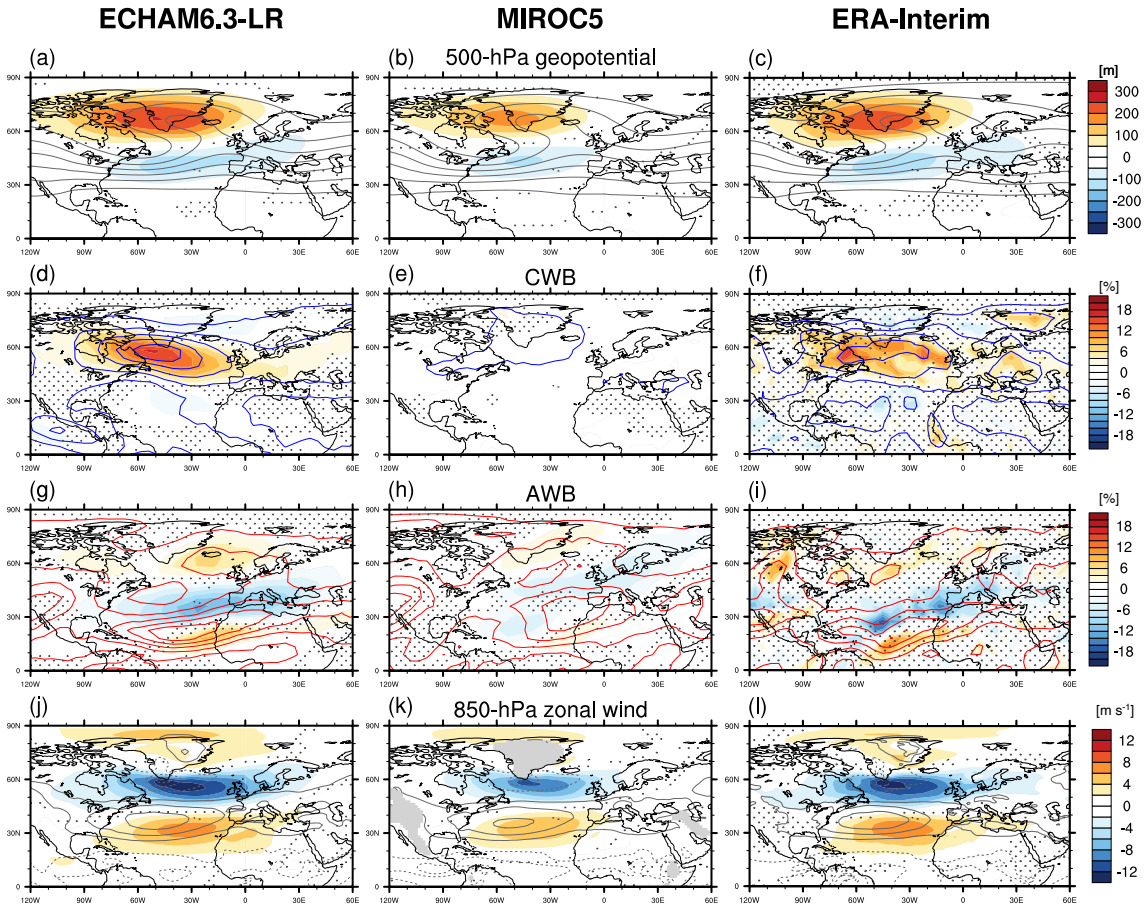

Figure 5. ~~Circulation~~ Ensemble means of the circulation anomalies during GB days for (left) ECHAM6.3-LR, (centre) MIROC5, and (right) ERA-Interim. (a,b,c) 500-hPa geopotential (contours are drawn every 100 m from 5000 to 6000 m) and anomalies (shading, in m). (d,e,f) Cyclonic wave breaking frequency (first contour and interval: 5%) and anomalies (shading, in %). (g,h,i) Same as (d,e,f) but for anticyclonic wave breaking frequency. (j,k,l) Zonal wind at 850 (first contour and interval: 4 m s^{-1}, zero contour omitted and dashed contours for negative values) and anomalies (shading, in m s^{-1}). Anomalies are deviations from the 10-year DJF climatology and only members with at least one blocked day are used for the composites. Dotted areas are not significant at the 10% level with the significance calculated using a bootstrap method.

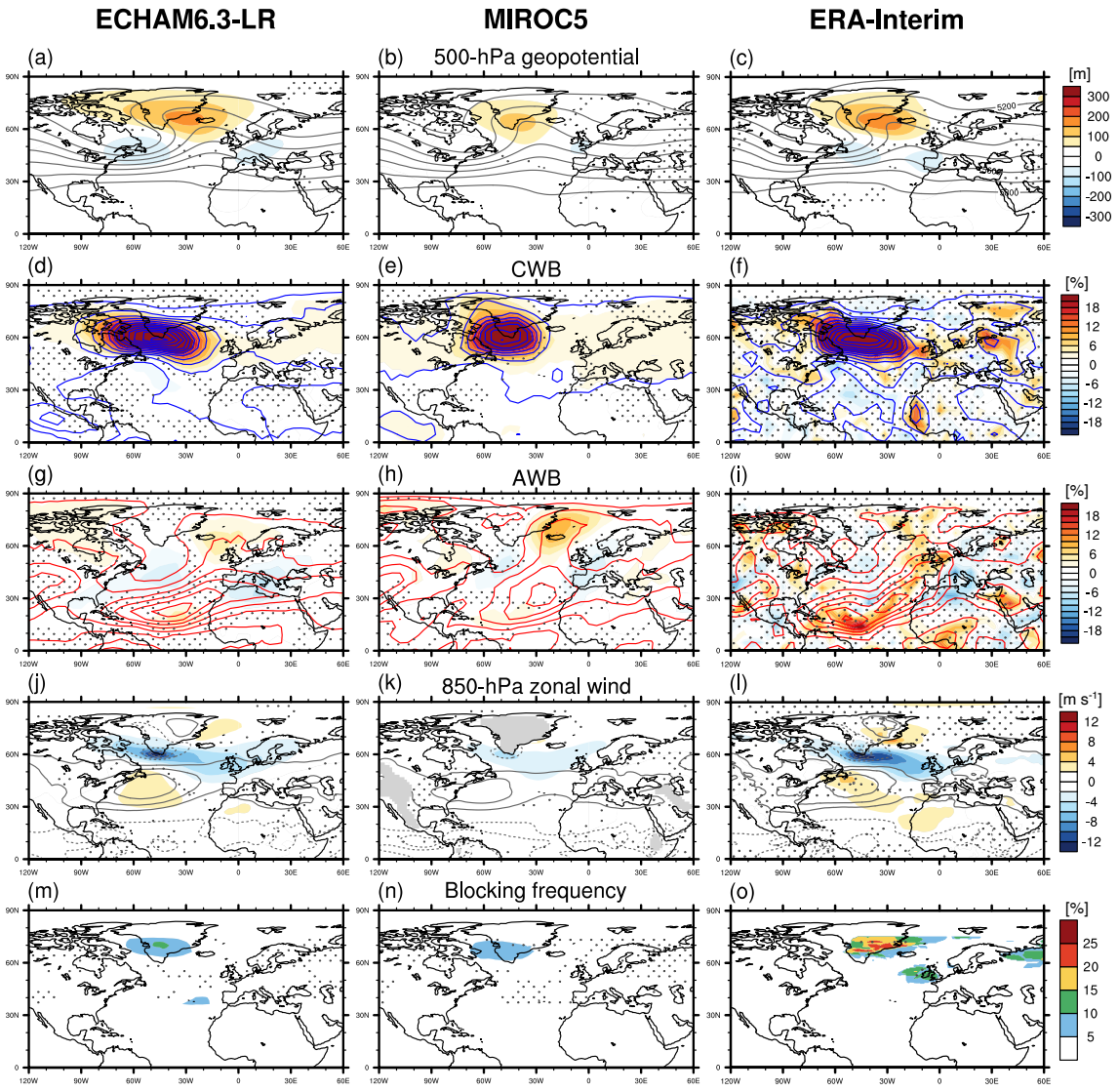

Figure 6. ~~Circulation~~ Ensemble means of the circulation anomalies during CWB days for (left) ECHAM6.3-LR, (centre) MIROC5, and (right) ERA-Interim. (a,b,c) 500-hPa geopotential (contours are drawn every 100 m from 5000 to 6000 m) and anomalies (shading, in m). (d,e,f) Cyclonic wave breaking frequency (first contour and interval: ~~0.05 day^{-1}~~5%) and anomalies (shading, ~~unit: day^{-1}~~in %). (g,h,i) Same as (c,d) but for anticyclonic wave breaking frequency. (j,k,l) Zonal wind at 850 hPa (first contour and interval: 4 m s^{-1}, zero contour omitted and dashed contours for negative values) and anomalies (shading, in m s^{-1}). (m,n,o) Blocking frequency (unit: fraction of the time with CWB). Dotted areas are not significant at the 10% level with the significance calculated using a bootstrap method.

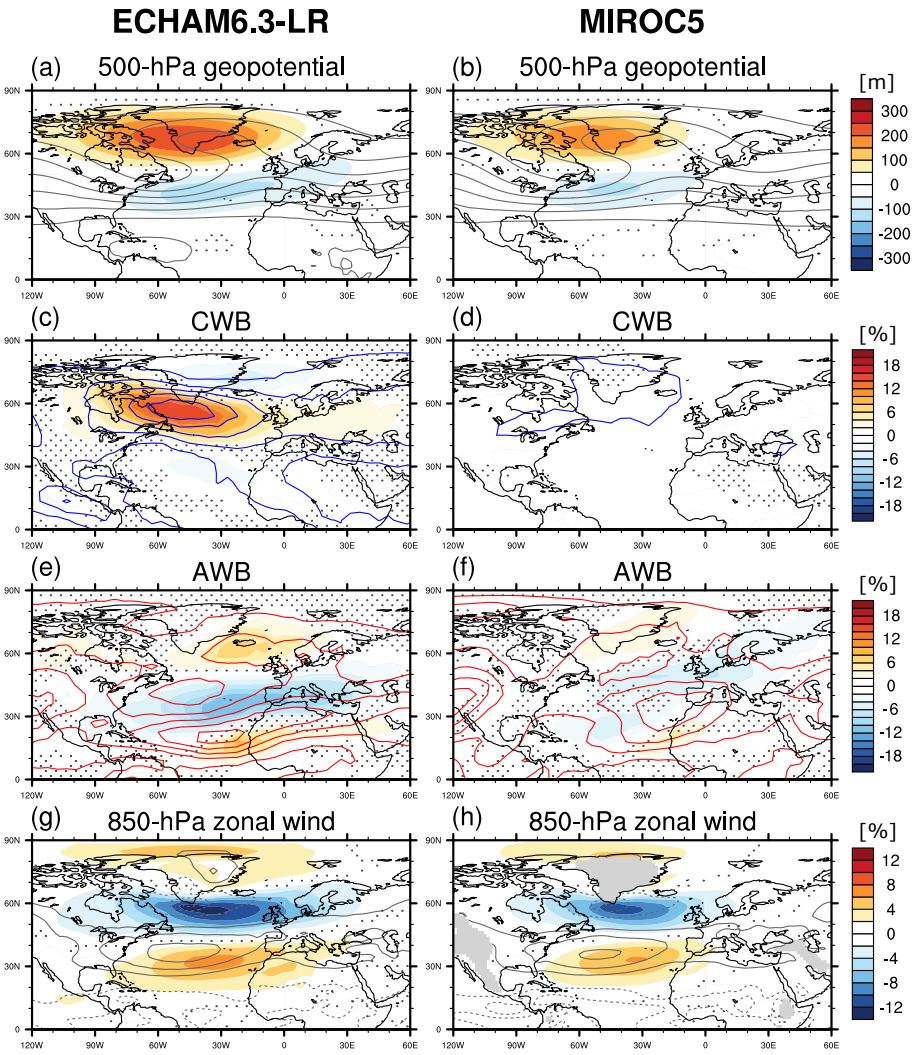

Figure 7. ~~Circulation~~ Ensemble means of the circulation anomalies during Greenland blocking days for (left) ECHAM6.3-LR and (right) MIROC5 future experiments. (a,b) 500-hPa geopotential (contours are drawn every 100 m from 5000 to 6000 m) and anomalies (shading, in m). (c,d) Cyclonic wave breaking frequency (first contour and interval: ~~0.05 day^{-1}~~ 5%) and anomalies (shading, ~~unit: day^{-1}~~ in %). (e,f) Same as (c,d) but for anticyclonic wave breaking frequency. (g,h) Zonal wind at 850 hPa (first contour and interval: 4 m s^{-1}, zero contour omitted~~and~~ , dashed contours for negative values) and anomalies (shading, in m s^{-1}). Anomalies are deviations from the 10-year DJF climatology and only members with at least one blocked day are used for the composites. Dotted areas are not significant at the 10% level with the significance calculated using a bootstrap method.

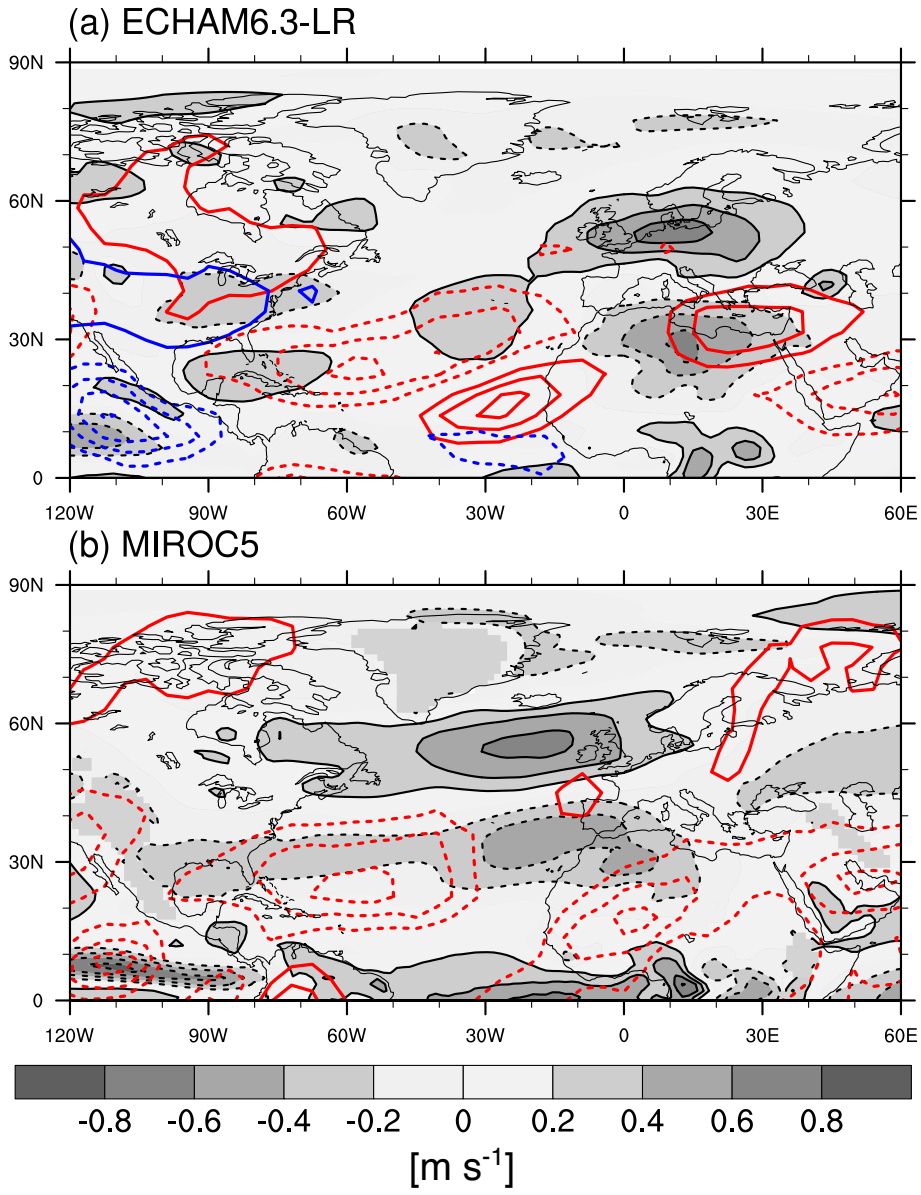

Figure 8. DJF ensemble mean responses (Future minus Present) of the Rossby wave frequency and 850-hPa zonal wind for (a) ECHAM6.3-LR and (b) MIROC5. Blue (red) contours show the responses for the (anti)cyclonic wave breaking frequency (first contour and interval: 0.005 day $^{-1}$). The gray shading and black contours show the response of the 850-hPa zonal wind (in m s^{-1}). The zero contours are omitted and dashed contours represent negative values.